EUROPEAN ORGANIZATION FOR NUCLEAR RESEARCH

Proposal to the ISOLDE and Neutron Time-of-Flight Committee

Laser Spectroscopy of exotic indium ($Z = 49$) isotopes: Approaching the $N = 50$ and $N = 82$ neutron numbers

January 7, 2017

R.F. Garcia Ruiz[1], C.L Binnersley[1], J. Billowes[1], M.L. Bissell[1], T.E. Cocolios[2], R.P. de Groote[2], G.J. Farooq-Smith[2], K.T. Flanagan[1], S. Franchoo[3], G. Hagen[4,5], A. Koszorús[2], K.M. Lynch[6], B.A. Marsh[7], G. Neyens[2], H.H. Stroke[8], A.R. Vernon[1], K. Wendt[9], S.G Wilkins[1], Z. Xu[4], X.F. Yang[4], D.T. Yordanov[3]

[1]*School of Physics and Astronomy, The University of Manchester, Manchester, M13 9PL, UK*
[2]*KU Leuven, Instituut voor Kern- en Stralingsfysica, B-3001 Leuven, Belgium*
[3]*Institut de Physique Nucleaire Orsay, IN2P3/CNRS, 91405 Orsay Cedex, France*
[4]*Physics Division, Oak Ridge National Laboratory, Oak Ridge, TN 37831, USA*
[5]*Department of Physics and Astronomy, University of Tennessee, Knoxville, TN 37996, USA*
[6]*Physics Department, CERN, CH-1211 Geneva 23, Switzerland*
[7]*Experimental Physics Department, CERN, CH-1211 Geneva 23, Switzerland*
[8]*Department of Physics, New York University, New York, New York 10003, USA*
[9]*Institut für Physik, Johannes Gutenberg-Universität, D-55128 Mainz, Germany*

Spokesperson:[Ronald Garcia Ruiz] [ronald.fernando.garcia.ruiz@cern.ch]
Contact person:[Kara M. Lynch] [kara.marie.lynch@cern.ch]

Abstract: The ground-state properties of exotic indium isotopes approaching the neutron numbers $N = 50$ and $N = 82$ will be studied by laser spectroscopy. Nuclear spins, changes in the rms charge radii and electromagnetic moments of $^{100-134}_{49}$In are proposed to be measured by collinear resonant ionization spectroscopy using the CRIS experimental beam line. The isotopes in the neighborhood of the so-called doubly-magic isotopes; $^{100}_{50}$Sn and $^{132}_{50}$Sn, are of particular interest for the recent developments on many-body methods and inter-nucleon interactions.

Requested shifts: 38 shifts distributed in 2 runs.

1 Motivation

The importance of nuclear structure studies approaching the $Z = N = 50$ and $N = 82$ shell closures has been widely recognized from both experiment and theory [1–9]. In spite of the great interest, our experimental knowledge of these nuclei is still rather poor, and several questions remain open in our understanding of the nuclear structure in the vicinity of $N = Z = 50$ [3,10–14] and $N = 82$ [1, 15–17]. Active experiments and recent proposals at ISOLDE such as IS524, IS538, IS548, IS549, IS551, IS560, IS562, IS573, IS574, IS595, IS600, IS610, IS613, P-484, P-487 illustrate the current experimental interest in this frontier region of the nuclear chart.

From the theoretical side, significant progress on the study of this region has been achieved during the last few years. Based on inter-nucleon interactions derived from chiral effective field theory [18–20], and thanks to the new advance on many-body methods [21–25], several milestones have been reached towards the *ab-inito* description of heavy nuclei. Nuclear theory is now able to provide *ab-initio* computations of nuclear properties in the neighborhood of tin isotopes [26].

This proposal suggests additional motivations for the study of indium isotopes ($Z = 49$). With a proton-hole in $Z = 50$, these isotopes provide a compelling scenario to explore the evolution of nuclear properties between the $N = 50$ and $N = 82$ neutron numbers. Our renewed interest in these nuclei has been encouraged by recent developments in *ab-initio* calculations, which are now able to provide predictions of nuclear properties for indium isotopes around the $N = 50$ and $N = 82$ neutron numbers [26].

The available experimental data on the ground-state properties of indium isotopes is limited to the region between ^{104}In ($N = 55$) and ^{127}In ($N = 78$), where most of the information has been reported from laser-spectroscopy experiments [27]. The spins, magnetic moments, quadrupole moments and charge radii of ground-states and isomers are unknown below ^{105}In and above ^{127}In. Here, we propose the extension of these measurements down to ^{100}In ($N = 51$), and up to ^{134}In ($N = 85$). These results will provide a singular test to the importance of many-body correlations across the $N = 50$ and $N = 82$ shell-closures, and will constitute an important benchmark for the development of microscopic interactions and many-body methods.

1.1 Spins and electromagnetic moments

The experimentally known ground-state magnetic moments and quadrupole moments of indium isotopes are shown in Figure 1. Within a simplified shell-model description, the odd-even indium isotopes are expected to be dominated by a single-proton hole in the $\pi g_{9/2}$ orbit. As shown in Figure 1, this single-particle picture seems to be nicely illustrated by a fairly constant behaviour of the g-factor and quadrupole moments for isotopes with spin $9/2^+$. Whether or not this simple trend persists in the proximity of $N = 50$ and $N = 82$ is an open question that would provide an important insight into the robustness of these shell closures.

In contrast, the structure of odd-odd isotopes appears to be much more complex. Different spins for ground and isomeric states (1^+, 2^+, 3^+, 4^+, 5^+, 7^+, 8^+) can be formed by the coupling of a proton-hole with neutrons filling the $\nu d_{5/2}$, $\nu g_{7/2}$, $\nu d_{3/2}$ and $\nu h_{11/2}$ orbits. The structure of the isotopes towards $N = 50$ depends on the ordering of the $\nu d_{5/2}$-$\nu g_{7/2}$ neutron orbits, a topic that has been largely debated in the literature (see for example [11, 14, 29, 30, 30]). Direct spin assignments are essential to understand the assumed evolution of shell-model orbits in these nuclei. Moreover, several studies in this region depend on spin assumptions for the ground-state of In isotopes (see for example [3, 31]).

The large variety of nuclear isomers present in the indium isotopic chain allows for the study

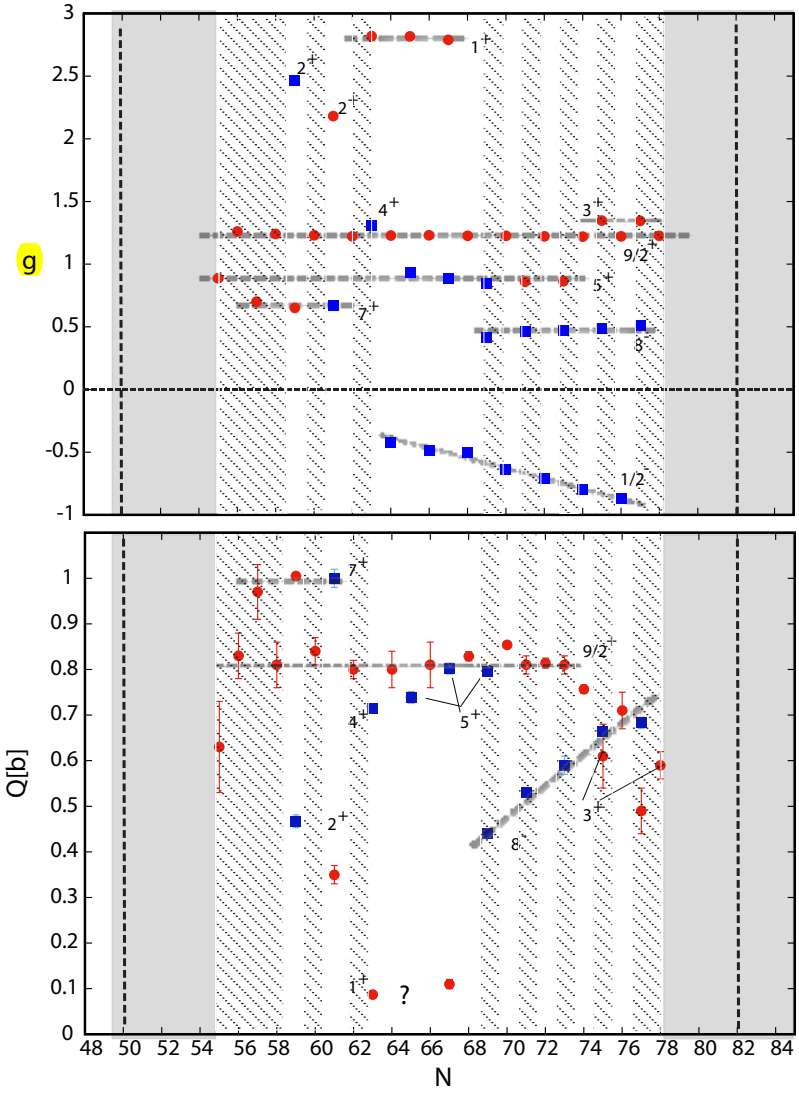

Figure 1: Experimental literature values for the g-factors ($g = \mu/(\mu_N I)$) (upper) and quadrupole (bottom) moments of In isotopes [28]. The electromagnetic-moments for the ground-state are shown in red color, and isomeric states in blue. Grey dotted lines connect isotopes with the same spin. Shaded areas highlight the regions where this proposal would provide new experimental information for both ground-state and isomers. Moreover, the spin, electromagnetic moments and charge radii are unknown for the isomers ^{104m,105m,106m,107m,109m_1,109m_2,111m,118m,120m,122m,124m,127m_1,127m_2}In (regions highlighted with diagonal lines).

of several aspects of nuclear structure such as the neutron-proton interaction [31], rare-decay modes from high-spin isomers [17], the evolution of collective motion [32], and the role of electro-weak currents in nuclear electromagnetic properties [31]. The odd-even isomers with $I = 1/2^-$, for example, appear to be dominated by a single proton in the $\pi p_{1/2}$ orbit, exhibiting a striking linear dependence of the magnetic moment (g-factors) with the neutron number (see Figure 1). When comparing electromagnetic moments with calculations, the deviation from the experimental values can be attributed either to missing configuration mixing and/or an incomplete description of the electromagnetic operators. As the magnetic moments of nuclei in $p_{1/2}$ orbits can be largely unaffected by configuration mixing [33], they are expected to be particularly sensitive to higher-order contributions to the $M1$ operator, e.g., two-body meson-exchange currents (MEC) [31]. Thus, the evolution of these $\pi p_{1/2}$ isomers across $N = 82$ would offer a unique scenario to study the role of electro-weak currents in the magnetic moments [31].

Chiral effective field theory allows a systematic and consistent treatment for the inclusion of electro-weak currents in electromagnetic operators (see for example [34, 35] and references therein). *Ab-initio* calculations with electro-weak currents derived from chiral effective field theory have shown that MEC produce large contributions to the magnetic moments (up to 40%) of light nuclei [35]. Efforts to extend the inclusion of electro-weak currents in coupled-cluster calculations for medium- and heavy-mass nuclei are underway [36]. Furthermore, recent developments on the shell-model in-medium similarity renormalization group have extended the connection of shell-models with *ab-initio* methods, expanding the *ab-inito* approach to open-shell nuclei [37]. Similar valence-space interactions are being develop in the Sn region [26]. In this approach, all operators can be treated on equal footing, allowing a consistent treatment of electromagnetic operators. Work is in progress to include electro-weak currents in the calculations of electromagnetic properties [38].

The developments on *ab-initio* methods and the consistent inclusion of electro-weak currents are expected to provide a new insight in our understanding of the nuclear dynamics, e.g., , to understand the microscopic origin of the commonly used effective charges of nucleons and quenching of g-factors [34, 35]. It is not only critical for a consistent description of electromagnetic properties, but has direct implications in our interpretation of the non-observable shell-structure associated to the atomic nucleus [39, 40].

To reinforce the relevance of the proposed studies in the development of many-body methods and inter-nucleon interactions, Figure 2 shows some preliminary results from *ab-initio* calculations for the energy levels of ^{100}In [26]. The calculations show the results from a novel charge exchange coupled-cluster equation-of-motion method using the NN+3NFs chiral interaction 1.8/2.0 (EM) [20]. It is worth to notice that this interaction was fitted only to nucleon-nucleon scattering data and binding energies and radii of $A = 3, 4$ nuclei [20]. Remarkably, the calculations are in good agreement with the observed 1^+ state [3], and predict a ground-state spin 7^+, which contrast with previous experimental results that suggested a ground-state spin 6^+ based on large-scale shell model calculations [3]. Unambiguous spin assignments are needed to clarify these suggestions. The additional challenges related to charge radii calculations and their sensitive to details of the inter-nucleon interactions are discussed in the following section.

1.2 Charge radii

The experimental charge radii known for isotopes with proton numbers around $Z = 50$ are shown in Figure 3. The charge radii evolution for indium isotopes has been interpreted as the

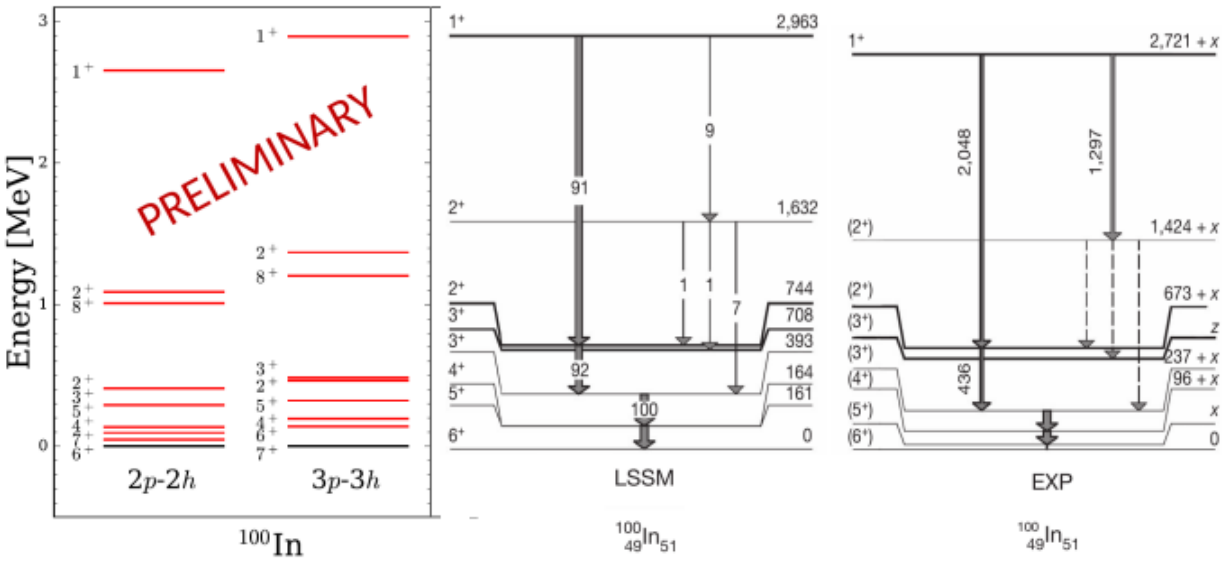

Figure 2: *Ab-initio* calculations for the energy levels of ^{100}In, compared with large-scale shell-model calculations (LLSM) and experimental results from Ref. [3]. *Ab-initio* calculations have been performed using a novel charge exchange coupled-cluster equation-of-motion method [26].

interplay between static deformation and larger dynamic surface correlations [32]. No experimental information has been reported for isotopes around $N = 50$ and across $N = 82$. Charge radii measurements combined with the results for electromagnetic moments will shed light on the evolution of static and dynamic collectivity around $N = 50$ and $N = 82$ [17, 31, 32, 41].
For *ab-initio* approaches, the simultaneous reproduction of binding energies and charge radii has been recognized as a long standing problem in the development of chiral interactions [43–45]. Recently, *ab-initio* calculations have shown that charge radii are highly sensitive to details of the inter-nucleon interactions, which up to now can not be constrained only by the properties of few-nucleon systems [43–45]. Figure 3 shows *ab-initio* calculations using different chiral interactions for binding energies and charge radii of selected nuclei up to ^{56}Ni. Although some chiral interactions provide a good description of binding energies, e.g., 1.8/2.0 (EM) [20], they exhibit clear deficiencies in the calculations of charge radii [25]. This problem was recently addressed by including ground state energies and charge radii of selected carbon and oxygen isotopes in the optimization of the chiral interaction. The resulting interaction, labeled as NNLO$_{\rm sat}$ [43], has provided a relatively good description of charge radii up to Ni isotopes [25] (see Figure 3). The extension of these calculations to the Sn region is ongoing [24].

In summary, the results expected from this proposal will provide the unknown spin, electromagnetic moments and changes in the rms charge radii for the ground and isomeric states of the isotopes $^{100-103}$In and $^{128-134}$In. (see Table 1). These ground-state properties will provide key information to understand the robustness of the $N = 50$ and $N = 82$ shell closures, and will serve as an important test to recent developments on many-body methods and inter-nucleon interactions. The extension of these measurements across the unknown isomers, ^{104m,105m,106m,107m,109m_1,109m_2,111m,118m,120m,122m,124m,127m_1,127m_2}In, will complete a comprehen-

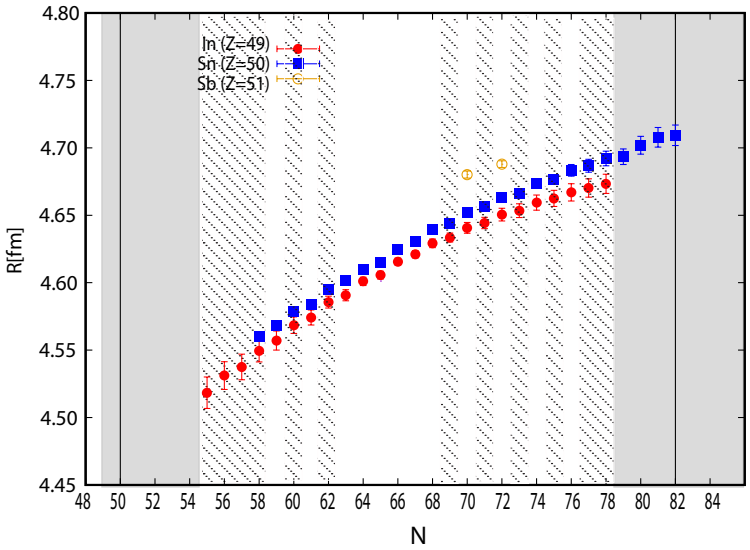

Figure 3: Experimental charge radii of isotopes in the neighborhood of tin isotopes [32, 42]. Shaded areas highlight the regions where this proposal would provide new experimental information for both ground-state and isomers. Moreover, the spin, electromagnetic moments and charge radii are unknown for the isomers ^{104m,105m,106m,107m,109m_1,109m_2,111m,118m,120m,122m,124m,127m_1,127m_2}In (regions highlighted with diagonal lines).

sive survey of the evolution of collectivity and proton-neutron interactions in the indium isotopic chain. Furthermore, the $\pi p_{1/2}$ isomers will offer a sensitive probe to test the role of electro-weak currents in the description of nuclear electromagnetic properties.

2 Experimental details

The experiments will be performed by using the collinear resonance ionization laser spectroscopy experiment (CRIS) at ISOLDE [46]. Measurements of the hyperfine structure spectra (hfs) and isotope shifts on the indium atom (In I) will provide the ground-state properties of exotic indium isotopes.
The HRS separator will be used in combination with the cooler-buncher ISCOOL. Bunches of singly-ionized indium ions (In II) will be redirected into the CRIS beam line. At CRIS, the ions are neutralized by using a charge exchange cell (CEC), and overlap with several laser beams in a collinear geometry along a UHV interaction region (1.2 m). A narrow-band laser can be used to resonantly excite the atomic transition of interest, and subsequently, a broad-band laser is used to ionize the atomic state into a In II state. The resonantly-ionized ions are then separated from the non-interacting atoms via electrostatic deflector plates and detected by an MCP particle detector.

The production of exotic indium isotopes is highly favored at ISOLDE. Indium isotopes can be produce by surface ionization and enhanced by the use of the resonance ionization ion source (RILIS) [47]. The reported yields at PSB are shown in Figure 1. A low-contamination is

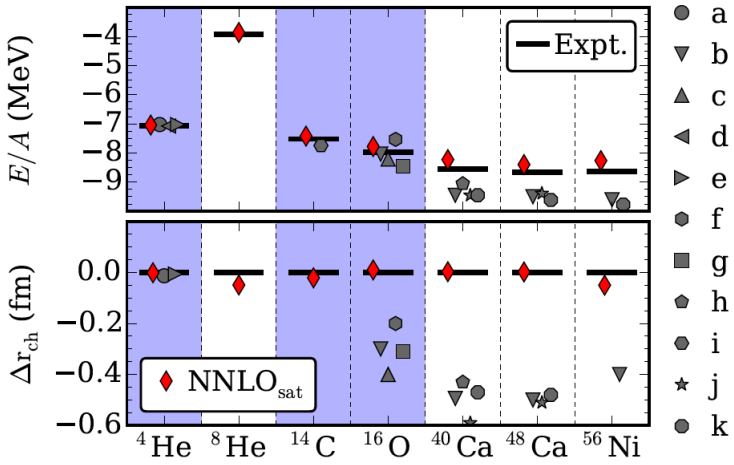

Figure 4: Ground-state energies per nucleon (top). The red diamonds show the *ab-initio* calculations with the newly developed chiral interaction $\mathrm{NNLO_{sat}}$ [43]. On the bottom the differences between calculations and experimental charge radii (bottom). While several interactions can provide a relatively good description of binding energies, the reproduction of charge radii has been a major challenge in the development of chiral Hamiltonians [23, 43–45]. As there is not experimental information for the charge radii of ^{56}Ni, the experimental charge radii of ^{58}Ni is used for comparison. Figure was taken from Ref. [25].

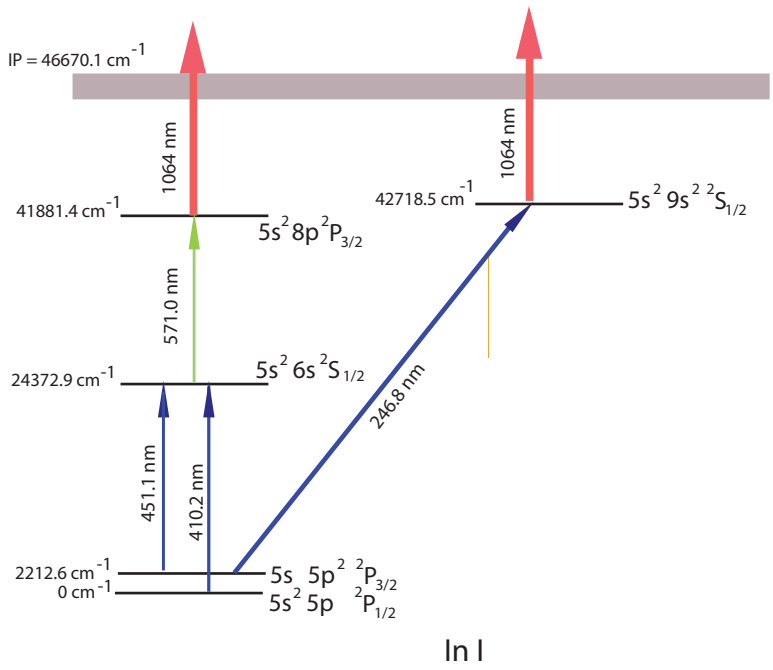

Figure 5: Possible resonance ionization schemes proposed for the study of In isotopes [51].

expected for neutron-deficient isotopes. On the neutron-rich side, a neutron converter can be used to suppress the Cs contamination [48]. Recently, experiments at the Isolde decay station confirmed the yields and high supression of Cs contaminants [49, 50]. Furthermore, the CRIS setup will suppress the Cs contaminants by a factor of more than 10^6, as demonstrated by the recent measurements of ^{78}Cu that detected a background rate of ^{78}Ga ($\sim 10^5$ ions/s) of only 1 count in 400 s.

2.1 Laser setup

The proposed resonant ionization schemes for the study of indium isotopes are shown in Figure 5. The atomic transitions at 451.1 nm and 410.2 nm were studied previously [27]. As the population of the meta-stable state $5s\ 5p^2\ ^2P_{3/2}$ is favored in the charge-exchange process, the transitions 451.1 nm is preferred for the proposed studies. Moreover, this transition was shown to be sensitive to the nuclear spins, gs electromagnetic moments and changes in the rms charge radii [27]. An alternative ionization path using the 246.8 nm line that could provide higher sensitivity will be tested off-line.

An injection seeded laser system recently installed at CRIS [52] can be used to provide the narrow band laser light at 451.1 nm (frequency doubled) or 246.8 nm (frequency tripled). A high power broad-band dye laser will be used to provide the required second step at 571.0 nm. The non-resonant ionization step (1064 nm) can be obtained from a high-power Nd:YAG laser (200 Hz).

3 Beam-time request

The experiments will be divided in two experimental campaigns; i) study of neutron-deficient isotopes using a LaC_x target, and ii) study of neutron-rich isotopes, which requires a UC_x target.
The yield of the most exotic isotope proposed in this study, ^{100}In, is of about 16 ions/s. Such isotope can be reached within the current sensitivity achieved at the CRIS setup. Recent experiments performed on Cu isotopes produced at rates of ∼30 ions/s [53], have shown the high-efficiency and high-resolution achieved at CRIS. Although the sensitivity in collinear laser spectroscopy is strongly element-dependent, the relatively long life-time (7 s) and the low-contamination expected at mass $A = 100$, will further assists the measurement of this isotope. All the other cases proposed in this study are produced with more than 10^2 ions/s and are expected to be relatively straight forward to measure.

The details of the beam production and the required shifts for this experimental proposal are summarized in Table 1. The required shifts were estimated assuming an overall efficiency of 0.3%. This conservative value is calculated assuming 30% transport and detection efficiency, 1.7% population of metastable hyperfine atomic state (10% neutralization distributed in 6 peaks), and 10 % laser ionization efficiency. For the most exotic case, ^{100}In, scans of about 3 minutes per step are required to obtain a signal with $> 5\sigma$ signal-to-background ratio. Therefore, a complete scan over a 10 GHz region using high-resolution steps (∼10 MHz) will take 6 shifts (3 min $\times 10^3$). For isotopes produced with yields higher than 10^3 ions/s, the time per scan is limited by the laser stabilization system. Once the laser frequency is changed, the laser stabilization takes ∼5 seconds to lock around the new frequency value. Thus, the time for scanning a 10 GHz region (10^3) is estimated to be 2-3 hours (0.3 shifts).
The required shifts for each isotope include the time for: i) scan the complete hyperfine structure spectrum, ii) the search of isomeric states, and iii) reference measurements to monitor the stability of the ion beam energy and systematic errors. For neutron-rich isotopes a contamination of Cs isotopes of about 10^2 orders of magnitude higher than the respective yields reported for In was assumed.

Summary of requested shifts: 38 shifts are required, distributed in two runs of 18.5 and 19.5 shifts, respectively.

References

[1] Jones, K. *et al. Nature* **465**, 454–457 (2010).

[2] Guastalla, G. *et al. Phys. Rev. Lett.* **110**, 172501 (2013).

[3] Hinke, C. *et al. Nature* **486**, 341–345 (2012).

[4] Faestermann, T., Górskab, M. & Grawe, H. *Prog. Part. Nucl. Phys.* **69**, 85–130 (2013).

[5] Allmond, J. M. *et al. Phys. Rev. Lett.* **112**, 172701 (2014).

[6] Simpson, G. *et al. Phys. Rev. Lett.* **113**, 132502 (2014).

[7] Lorusso, G. *et al. Phys. Rev. Lett.* **114**, 192501 (2015).

Isotope	I (Tentative)	Half life	Yield (ions/s)	Target+RILIS	Shifts
^{100}In	$(6^+, 7^+)$	7.0 s	16	LaC_x	6
^{101}In	$(9/2^+)$	15 s	380	LaC_x	2
^{102}In	(6^+)	22 s	8.6×10^3	LaC_x	0.5
^{103}In	$(9/2^+)$	65 s	8.0×10^4	LaC_x	0.5
^{103m}In	$(1/2^-)$	34 s	$>10^2$	LaC_x	1
^{104m}In	(3^+)	15.7 s	$>10^2$	LaC_x	1
^{105m}In	$(1/2^-)$	48 s	$>10^4$	LaC_x	0.3
^{106m}In	(2^+)	5.2 m	$>10^4$	LaC_x	0.3
^{107m}In	$(1/2^+)$	50.4 s	$>10^5$	LaC_x	0.3
^{109m_1}In	$(1/2^-)$	1.34 m	$>10^3$	LaC_x	0.3
^{109m_2}In	$(19/2^-)$	0.21 s	$>10^3$	LaC_x	0.3
^{111m}In	$(1/2^-)$	7.7 m	$>10^3$	LaC_x	0.3
^{118m}In	(1^+)	5.0 s	$>10^5$	LaC_x	0.3
^{120m}In	(1^+)	3.1 s	$>10^4$	LaC_x	0.3
^{122m}In	(1^+)	1.5 s	$>10^2$	LaC_x	1
$^{112-122}$In	–	>1 s	$\geq 10^4$	LaC_x	4
$^{112-122}$In	–	>1 s	$\geq 10^4$	UC_x	4[i]
^{124m}In	(1^+)	3.1 s	$>10^2$	UC_x	0.5
^{127m_1}In	$(1/2^-)$	3.7 s	$>10^2$	UC_x	0.5
^{127m_2}In	(21^+)	1.0 s	$>10^2$	UC_x	0.5
^{128}In	(3^+)	0.84 s	8.8×10^3	UC_x	0.5
^{128m}In	(8^-)	0.72 s	$>10^2$	UC_x	1
^{129}In	$(9/2^+)$	0.61 s	2.2×10^3	UC_x	0.5
^{129m_1}In	$(1/2^-)$	1.23 s	$>10^2$	UC_x	1
^{129m_2}In	$(23/2^-)$	0.67 s	$>10^2$	UC_x	1
^{130}In	(1^-)	0.29 s	$>10^3$	UC_x	0.5
^{130m_1}In	(10^-)	0.54 s	$>10^2$	UC_x	1
^{130m_2}In	(5^+)	0.54 s	$>10^2$	UC_x	1
^{131}In	$(9/2^+)$	0.28 s	$>10^3$	UC_x	0.5
^{131m_1}In	$(1/2^-)$	0.35 s	$>10^2$	UC_x	1
^{131m_2}In	$(21/2^+)$	0.32 s	$>10^2$	UC_x	1
^{132}In	(7^-)	0.20 s	1.6×10^4	UC_x	0.5
^{133}In	$(9/2^+)$	165 ms	1.8×10^3	UC_x	0.5
^{133m_1}In	$(1/2^-)$	180 ms	$>10^2$	UC_x	1
^{134}In	$(4^-$ to $7^-)$	138 ms	190	UC_x	3

Table 1: Table of reported yields and beam time request. Beam intensities correspond to 2 μA of average proton current at 1.4 GeV [47, 54]. Yields for isomeric states are estimated assuming a production of two orders of magnitude less than the yield reported for the respective ground-state [27]. Spin, electromagnetic moments and changes in the rms charge radii are unknown for these isotopes. [i]Measurements of stable isotopes are needed for voltage calibrations and extraction of isotope shifts.

[8] Bader, V. *et al. Phys. Rev. C* **88**, 051301(R) (2013).

[9] Coraggio, L. *et al. Phys. Rev. C* **91**, 041301(R) (2015).

[10] Banu, A. *et al. Phys. Rev. C* **71**, 061305(R) (2005).

[11] Vaman, C. *et al. Phys. Rev. Lett.* **99**, 162501 (2007).

[12] Doornenbal, P. *et al. Phys. Rev. C* **90**, 061302(R) (2014).

[13] Allmond, J. *et al. Phys. Rev. C* **92**, 041303(R) (2015).

[14] Ekström, A. *et al. Phys. Rev. Lett.* **101**, 012502 (2008).

[15] Dworschak, M. *et al. Phys. Rev. Lett.* **100**, 072501 (2008).

[16] Taprogge, J. *et al. Phys. Rev. Lett.* **112**, 132501 (2014).

[17] Yuan, C. *et al. Phys. Lett. B* **762**, 237 (2016).

[18] Epelbaum, E., Hammer, H.-W. & Meißner, U.-G. *Rev. Mod. Phys.* **81**, 1773–1825 (2009).

[19] Hammer, H.-W., Nogga, A. & Schwenk, A. *Rev. Mod. Phys.* **85**, 197 (2013).

[20] Hebeler, K. *et al. Phys. Rev. C* **83**, 031301(R) (2011).

[21] Hagen, G., Hjorth-Jensen, M., Jansen, G. R., Machleidt, R. & Papenbrock, T. *Phys. Rev. Lett.* **109**, 032502 (2012).

[22] Somà, V., Cipollone, A., Barbieri, C., Navrátil, P. & Duguet, T. *Phys. Rev. C* **89**, 061301 (2014).

[23] Binder, S., Langhammer, J., Calci, A. & Roth, R. *Phys. Lett. B* **736**, 119 (2014).

[24] Binder, S., Ekström, A., Hagen, G., Papenbrock, T. & Wendt, K. A. *Phys. Rev. C* **93**, 044332 (2016).

[25] Hagen, G., Hjorth-Jensen, M., Jansen, G. & Papenbrock, T. *Physica Scripta* **91**, 063006 (2016).

[26] Hagen, G. *et al.* In preparation (2017).

[27] Eberz, J. *et al. Nucl. Phys. A* **464**, 9 (1987).

[28] Stone, N. J. *Atomic Data And Nuclear Data Tables* **90**, 75–176 (2005).

[29] Seweryniak, D. *et al. Phys. Rev. Lett.* **99**, 022504 (2007).

[30] Darby, I. G. *et al. Phys. Rev. Lett.* **105**, 162502 (2010).

[31] Rejmund, M. *et al. Physics Letters B* **753**, 86 – 90 (2016).

[32] Eberz, J. *et al. Z. Phys.* **A326**, 121 (1987).

[33] Arima, A. & Horie, H. *Progress of Theoretical Physics* **12**, 623–641 (1954).

[34] Carlson, J. *et al. Rev. Mod. Phys.* **87**, 1067–1118 (2015).

[35] Pastore, S. *et al. Phys. Rev. C* **87**, 035503 (2013).

[36] Ekström, A. *et al. Phys. Rev. Lett.* **113**, 262504 (2014).

[37] Stroberg, S. *et al. Accepted in Phys. Rev. Lett.* (2017).

[38] Holt, J. *Private communication* (2017).

[39] Maheshwari, B., Jain, A. K. & Srivastava, P. C. *Phys. Rev. C* **91**, 024321 (2015).

[40] Lică, R. *et al. Phys. Rev. C* **93**, 044303 (2016).

[41] Van Maldeghem, J., Heyde, K. & Sau, J. *Phys. Rev. C* **32**, 1067–1075 (1985). URL `http://link.aps.org/doi/10.1103/PhysRevC.32.1067`.

[42] Fricke, G. & Heilig, K. *Nuclear Charge Radii* (Springer, 2004).

[43] Ekström, A. *et al. Phys. Rev. C* **91**, 051301 (2015).

[44] Hagen, G. *et al. Nature Physics* **12**, 186 (2016).

[45] Garcia Ruiz, R. F. *et al. Nature Physics* **12**, 594 (2016).

[46] Cocolios, T. E. *et al. Nucl. Inst. Meth. B* **376**, 284 (2016).

[47] Köster, U. *et al. Nucl. Inst. Meth. B* **266**, 4229–4239 (2008).

[48] Dillman, I. *et al. Eur. Phys. J* **A12**, 281 (2002).

[49] Fraile, L. & Winther, A. *CERN-INTC-2015-049* **INTC-P-449** (2015).

[50] Lica, R. *Private communication* (2017).

[51] Kramida, A., Ralchenko, Y., Reader, J. & Team, N. A. *NIST Atomic Spectra Database* **(version 5.3)**, http://physics.nist.gov/asd (2015).

[52] Volker, S. Laser developments and high resolution resonance ionization spectroscopy of actinide elements. *PhD Thesis. University of Jyvskyl* (2015).

[53] de Groote, R. P. *et al. In preparation* (2017).

[54] ISOLDE. Indium isotopes. *YIELDS DATABASE* (YIELDS DATABASE). URL `http://test-isolde-yields.web.cern.ch`.

Appendix

DESCRIPTION OF THE PROPOSED EXPERIMENT

The experimental setup comprises: (*name the fixed-ISOLDE installations, as well as flexible elements of the experiment*)

Part of the	Availability	Design and manufacturing
CRIS	☒ Existing	☒ To be used without any modification
[Part 1 of experiment/ equipment]	☐ Existing	☐ To be used without any modification ☐ To be modified
	☐ New	☐ Standard equipment supplied by a manufacturer ☐ CERN/collaboration responsible for the design and/or manufacturing
[Part 2 of experiment/ equipment]	☐ Existing	☐ To be used without any modification ☐ To be modified
	☐ New	☐ Standard equipment supplied by a manufacturer ☐ CERN/collaboration responsible for the design and/or manufacturing
[insert lines if needed]		

HAZARDS GENERATED BY THE EXPERIMENT (if using fixed installation:) Hazards named in the document relevant for the fixed CRIS installation.

Additional hazards: no additional hazards

Hazards	[Part 1 of experiment/ equipment]	[Part 2 of experiment/ equipment]	[Part 3 of experiment/ equipment]
Thermodynamic and fluidic			
Pressure	[pressure][Bar], [volume][l]		
Vacuum			
Temperature	[temperature] [K]		
Heat transfer			
Thermal properties of materials			
Cryogenic fluid	[fluid], [pressure][Bar], [volume][l]		
Electrical and electromagnetic			
Electricity	[voltage] [V], [current][A]		
Static electricity			
Magnetic field	[magnetic field] [T]		
Batteries	☐		
Capacitors	☐		

Ionizing radiation			
Target material [material]			
Beam particle type (e, p, ions, etc)			
Beam intensity			
Beam energy			
Cooling liquids	[liquid]		
Gases	[gas]		
Calibration sources:	□		
• Open source	□		
• Sealed source	□ [ISO standard]		
• Isotope			
• Activity			
Use of activated material:			
• Description	□		
• Dose rate on contact and in 10 cm distance	[dose][mSV]		
• Isotope			
• Activity			
Non-ionizing radiation			
Laser			
UV light			
Microwaves (300MHz-30 GHz)			
Radiofrequency (1-300 MHz)			
Chemical			
Toxic	[chemical agent], [quantity]		
Harmful	[chem. agent], [quant.]		
CMR (carcinogens, mutagens and substances toxic to reproduction)	[chem. agent], [quant.]		
Corrosive	[chem. agent], [quant.]		
Irritant	[chem. agent], [quant.]		
Flammable	[chem. agent], [quant.]		
Oxidizing	[chem. agent], [quant.]		
Explosiveness	[chem. agent], [quant.]		
Asphyxiant	[chem. agent], [quant.]		
Dangerous for the environment	[chem. agent], [quant.]		
Mechanical			

Physical impact or mechanical energy (moving parts)	[location]		
Mechanical properties (Sharp, rough, slippery)	[location]		
Vibration	[location]		
Vehicles and Means of Transport	[location]		
Noise			
Frequency	[frequency],[Hz]		
Intensity			
Physical			
Confined spaces	[location]		
High workplaces	[location]		
Access to high workplaces	[location]		
Obstructions in passageways	[location]		
Manual handling	[location]		
Poor ergonomics	[location]		

Hazard identification:

Average electrical power requirements (excluding fixed ISOLDE-installation mentioned above): [make a rough estimate of the total power consumption of the additional equipment used in the experiment]